

ARTICLE

## Recent advances in batch production of transfer-free graphene

Ye Fang,<sup>ab‡</sup> Kaixuan Zhou,<sup>ab‡</sup> Wenze Wei,<sup>b</sup> Jincan Zhang,<sup>a\*</sup> and Jingyu Sun<sup>ab\*</sup>

Received 00th January 20xx,  
Accepted 00th January 20xx

DOI: 10.1039/x0xx00000x

Large-area transfer-free graphene film prepared via chemical vapor deposition has been proven appealing for various applications, with exciting demonstrations in electronics, photonics, and optoelectronics. To fulfil its commercialisation, batch production is a prerequisite. Nevertheless, the prevailing scalable synthetic strategies reported are still handicapped by production efficiency and uniformity. There has been also a lack of reviews in this realm. We present herein a comprehensive and timely summary in the recent advances of the batch production of transfer-free graphene. Primary issues and promising approaches to improve graphene growth rate are firstly addressed, followed by discussing the strategies to guarantee in-plane and batch uniformity for graphene grown on planar plates and wafer-scale substrates, with the design of target equipment to meet productivity requirements. Finally, potential research directions are outlined, aiming to offer insights in guiding the scalable production of transfer-free graphene.

### Introduction

Graphene, with its high carrier mobility,<sup>1</sup> high thermal conductivity,<sup>2-4</sup> and exceptional mechanical strength, is promising for applications in multiple fields including electronics and photonics.<sup>5</sup> In particular, the coating of graphene on various insulating substrates has attracted widespread interests because of the ability of graphene in bringing new possibilities for the application scenarios.<sup>6-8</sup> For instance, large-area graphene film directly grown on glass endows the conventional glass materials with new electrical and thermal conductive features, which enables emerging applications such as de-icing and de-fogging.<sup>9</sup> Graphene grown on wafer-scale sapphire substrates have offered advancements in the epitaxy of III-nitride materials, serving as a critical component in light-emitting diode (LED) devices for enhanced heat dissipation and illumination efficiency.<sup>10</sup> Nevertheless, commercialisation of such graphene-involved products is not possible until the batch production of graphene on these substrates is realized.

To date, different methodologies, including mechanical exfoliation, liquid-phase exfoliation, SiC epitaxy, and chemical vapor deposition (CVD), have been developed to prepare graphene materials.<sup>11-15</sup> However, most of them are not appropriate for controllable preparation of graphene on insulating substrates in a controllable manner.<sup>16-18</sup> For instance, the graphene obtained by mechanical

exfoliation harvests advanced quality, yet is limited by the small material productivity, which is normally suitable in laboratory-scale research. Liquid-phase exfoliation method could produce graphene in powdery form, where it remains difficult to control the layer numbers and impurity contents. Graphene oxide reduction suffers from high structural defects<sup>19</sup>; SiC epitaxy has the drawbacks regarding high cost aspect and singular substrate type.<sup>20</sup> In contrast, CVD method has emerged as a promising technique to produce large-area and high-quality graphene films, thanks to its fine controllability and scalability.<sup>21-24</sup> In this sense, direct growth of graphene on insulating substrates,<sup>25</sup> which readily eliminates complicate transfer process, exhibits high compatibility with practical application scenarios. Therefore, to meet the growing market demand, batch production of transfer-free graphene with advanced uniformity and cost-effectiveness is imperative.

Versatile tactics have been put forward to improving quality of transfer-free graphene, such as substrate design, carbon source selection,<sup>36</sup> and additive introduction.<sup>27-29</sup> However, these studies mainly employed growth samples affording limited sizes. Currently, to achieve batch production of graphene, there are primary challenges in four aspects: i) low preparation efficiency,<sup>28</sup> ii) lack of in-plane uniformity,<sup>30</sup> iii) poor uniformity within one batch,<sup>31</sup> and iv) lack of equipment suitable for mass production. Recent reviews have summarised either the synthesis of high-quality graphene on insulators<sup>6</sup> or the mass production of graphene on metal substrates.<sup>32</sup> Yet, there is no overview on the batch production of transfer-free graphene.<sup>6, 33-35</sup>

Herein, we summarise the recent advances in the batch production of large-area transfer-free graphene, aiming to comprehensively cover the state-of-the-art progresses and existing challenges (Figure 1). Starting from detailing the strategies in the promotion of graphene growth rate, case studies on the film uniformity of

<sup>a</sup> College of Energy, SUDA-BGI Collaborative Innovation Centre, Key Laboratory of Advanced Carbon Materials and Wearable Energy Technologies of Jiangsu Province, Soochow University, Suzhou 215006, China.

E-mail: sunjy86@suda.edu.cn (J. Sun); jczhang2024@suda.edu.cn (J. Zhang)

<sup>b</sup> Beijing Graphene Institute, Beijing 100095, China.

<sup>‡</sup>These authors contributed equally to this work.

graphene grown on both wafer and plate substrates are reviewed. Susceptor design to fulfil batch uniformity, together with optimised flow and thermal fields are then described, followed by discussing the equipment requirements towards mass production. Finally, our perspectives in the development of scalable synthesis strategies of transfer-free graphene are provided.

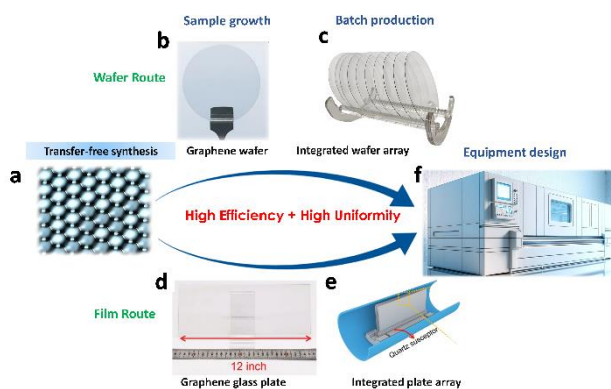


**Fig. 1** Pathways and targets for batch production of transfer-free graphene. (a) Schematic diagram of transfer-free synthesis of graphene. (b) A photograph showing a 2-inch-sized graphene/sapphire wafer. (c) Susceptor designed for batch production of graphene wafers. (d) A photograph showing a graphene glass plate. (e) Susceptor designed for batch production of graphene glass materials. (f) Schematic diagram of CVD equipment for scalable production of transfer-free graphene. (b) Reproduced with permission.<sup>36</sup> Copyright 2022, Science China Press. (d, e) Reproduced with permission.<sup>37</sup> Copyright 2023, Wiley-VCH.

## Rapid synthesis of transfer-free graphene

High production efficiency is critical to reduce the production cost of large-area transfer-free graphene films. Even though there are several factors influencing production efficiency, the major lies in the growth duration, which is normally quite lengthy (*i.e.*, 3–10 h).<sup>38–40</sup> Therefore, increasing the growth rate of graphene is the key to enhancing its efficiency. Methane is the most employed carbon precursor for CVD growth of graphene.<sup>41–44</sup> However, breaking its C–H bonding requires high energy without the presence of metal catalysts.<sup>45–47</sup> This results in low cracking rates of methane and thus limited supply of active carbon species for graphene directly grown on insulating substrates, and finally leading to the slow growth. To achieve rapid preparation of transfer-free graphene, elevating growth temperature and using precursors with lower pyrolysis barriers are effective.<sup>48–50</sup>

Increasing the growth temperature can significantly accelerate the cracking process of methane, thereby shortening the growth time of graphene. For instance, Fanton *et al.* proposed a method for preparing graphene under conditions exceedingly typically employed growth temperatures (1000 to 1150 °C). At such high temperatures of >1425 °C, methane completely decomposes, providing a large amount of active carbon source for graphene growth (Figure 2a).<sup>40</sup> As a result, the growth time of graphene was reduced to 1200 sec., allowing for the direct growth of continuous and high-quality graphene films on sapphire substrates (Figure 2b). However, at such high temperatures, the sapphire surface forms step edges with roughness reaching tens of nanometers,<sup>51, 52</sup> posing certain challenges for in-plane stitching of graphene domains. Chen *et al.* independently designed and built an ultra-high-temperature (up to 1600 °C) cold-wall CVD (CW-CVD) apparatus (Figure 2c).<sup>48</sup> By

controlling the graphene growth temperature in the range from 1350 to 1400 °C, the formation of excessively bumpy steps over the sapphire surface was effectively inhibited, where 2-inch-sized graphene/sapphire wafers were successfully produced (Figure 2d–2e). Moreover, since the high-temperature region is restricted to the substrate and its surface, the formation of amorphous carbon greatly restrained.<sup>53</sup>

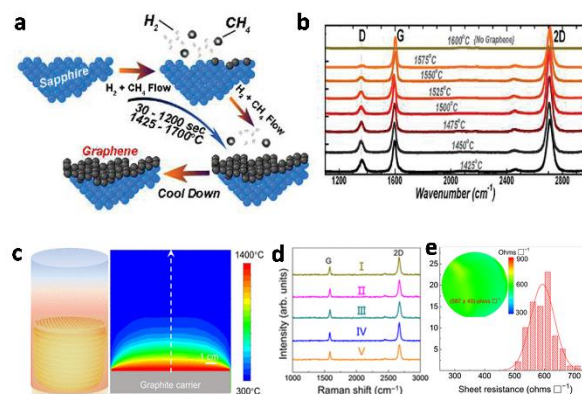


**Fig. 2** Rapid synthesis of transfer-free graphene films via elevating growth temperatures. (a) Schematic of graphene synthesis on sapphire at elevated temperatures. (b) Raman spectra of graphene grown on sapphire at temperatures ranging from 1425 to 1575 °C. (c) Schematic of the homemade electromagnetic induction heating CW-CVD reactor, where sapphire substrate is directly placed on the graphite carrier that is surrounded with induction coil (left panel), with the simulated temperature distribution inside the CVD system (at 1400 °C, 2000 Pa) (right panel). (d) Raman spectra of as-grown graphene measured at five randomly selected positions. (e) Histogram of sheet resistance values of a 2-inch-sized graphene/sapphire wafer. Inset: Sheet resistance mapping result. (a, b) Reproduced with permission.<sup>40</sup> Copyright 2011, American Chemical Society. (c–e) Reproduced with permission.<sup>48</sup> Copyright 2021, American Association for the Advancement of Science.

Using carbon sources with lower pyrolysis barriers (such as ethane,<sup>49</sup> acetylene,<sup>54, 55</sup> ethanol,<sup>56, 57</sup>) could also help shorten the preparation time of graphene, owing to significantly increased supply of active carbon species required for the growth. Sun *et al.* found that using ethane and methane as carbon sources, the growth rate ratio of graphene is about 4:1, which is mainly attributed to lower energy barrier required to break the C–C bonds in ethane (368 kJ/mol) than that to break C–H bonds in methane (431 kJ/mol).<sup>49</sup> This also contributes to a lower pyrolysis temperature for ethane, thus allowing the growth of graphene at 750 °C, far lower than the methane's case at 1000 °C (Figure 3a–3e). Chen *et al.* observed that the growth rate ratio of graphene on quartz substrate using ethanol and methane as the carbon sources reaches 20:1, owing to the lower cracking temperature and faster cracking rate of ethanol as compared to methane (Figure 3f). As a result, they acquired large-sized, uniform graphene glass samples within 4 min using ethanol as the carbon source.<sup>32</sup> Moreover, as the growth time extends, the thickness of graphene on the glass surface gradually increases, as evidenced by the gradually decreased transparency of the graphene/glass materials (Figure 3g). This would allow the synthesis of graphene with favourable uniformity (Figure 3h). However, more efforts are requested to further improve the quality of the directly grown graphene films.

## Large-area growth of transfer-free graphene

Currently, CVD growth of graphene films on insulating substrates in centimetre scale has been widely reported.<sup>58–60</sup> However, when increasing the sample size by several orders of magnitude, non-uniformity has emerged as a prominent issue, acting as the main hurdle towards practical applications. Strategies to fulfil large-area synthesis of transfer-free graphene films are highly related with the shape, size, and compositions of the target substrates, which can be classified into two types: sheet with sizes ranging from decimetre to meter and wafer with sizes ranging from 2 to 12 inches. The former mainly deals with glass substrates that could make the best of graphene's thermal and electrical features for applications such as transparent conductor and Joule heating,<sup>37, 61</sup> while the latter includes sapphire, quartz, and Si wafers that are commonly used in integrated electronics, photonics, and optoelectronics.<sup>26, 62–64</sup>

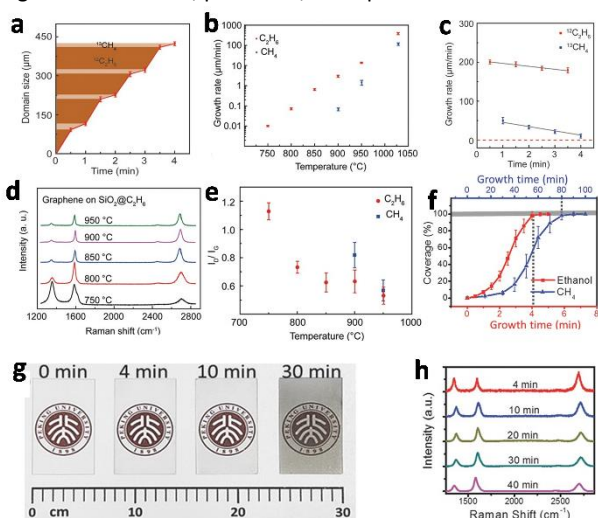


**Fig. 3** Rapid synthesis of transfer-free graphene films using carbon sources with lower cracking barriers. (a) Domain size (diagonal of graphene domains) of as-grown graphene as a function of growth time. (b) Growth rate of graphene as a function of growth temperature. (c) Growth rate of graphene as a function of growth time. (d) Raman spectra of graphene grown using ethanol at different temperatures. (e) Raman intensity ratio of D to G band ( $I_D/I_G$ ) of graphene grown using ethane or methane under different growth temperatures. (f) Coverage of graphene on glass as a function of growth time using ethanol (red) and methane (blue) precursors. (g) Photos of 10 cm  $\times$  6 cm-sized graphene/glass samples with growth times of 4, 10, and 30 min. (h) A series of Raman spectra of graphene films with growth times of 4, 10, 20, 30, and 40 min. (a–e) Reproduced with permission.<sup>49</sup> Copyright 2017, Wiley-VCH. (f–h) Reproduced with permission.<sup>32</sup> Copyright 2016, Wiley-VCH.

## Transfer-free growth on meter-sized glass substrates

As for the meter-sized glass plates, the key to advancing graphene uniformity is to ensure the homogeneous distribution of carbon species transport above substrates. Methane, as mentioned above, has a high cracking temperature and slow cracking rate, normally leading to uneven distribution of active carbons and thus non-uniform thickness of grown graphene films.<sup>65, 66</sup> This phenomenon is particularly evident in the CVD preparation of large-sized graphene materials on insulators, especially when growing under atmospheric pressure. Several strategies have been proposed to solve this issue, which differs according to the substrate types.

Quartz glass is known for its excellent chemical stability, high mechanical strength, and high transparency. Combining graphene

with quartz could integrate the conductivity of graphene with the transparency of glass, leading to the development of next-generation optical devices.<sup>67</sup> Pressure control is an easy way to improve uniformity of transfer-free graphene directly grown on glass substrate, thanks to a more uniform distribution of active carbon species under a lower pressure. However, only limited improvement can be achieved in this sense. Special design inside the CVD chamber is another strategy to adjust the distribution of carbon sources.<sup>68, 69</sup> However, this is not highly compatible with batch production process. The most effective strategy to date lies in replacing methane by other types of carbon sources that have lower decomposition barriers. For instance, the lower cracking temperature and faster cracking rate makes ethanol a good candidate to grow uniform graphene on quartz glass in a low-pressure environment, because of the significantly improved mass transfer and uniform active carbon distribution within the growth regime (Figure 4a–4e). Moreover, lower pressure leads to fewer gas collisions, higher mass transfer coefficient, and lower carbon species concentration, all of which contribute to inhibiting the formation of amorphous carbon. Similarly, gas-phase additive is also beneficial to the uniformity of large-area graphene growth, as demonstrated by Liu et al. in employing hydroxyl species in situ released from the quartz substrates for producing 12-inch  $\times$  4-inch-sized high-quality graphene/quartz glass materials (Figure 4f–4h).

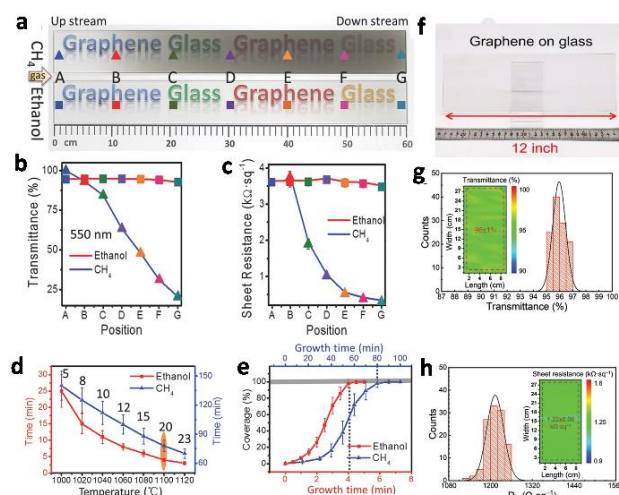


**Fig. 4** Direct growth of large-area graphene films on glass substrates. (a) Photograph of 25-inch-sized graphene/glass samples grown using methane-precursor-based APCVD (upper panel) and ethanol-precursor-based LPCVD (lower panel). (b, c) Differences in the transmittance (b) and sheet resistance (c) of the graphene samples synthesized using methane (triangles) and ethanol (squares) precursors. (d) Time requirement for growing graphene with full coverage on glass via the two synthesis routes at temperatures from 1000 to 1120 °C. The numbers above the curves (5–23) represent the improvement of the growth efficiency. (e) Growth-time dependence of the graphene glass samples synthesised through the ethanol-precursor-based (red) and methane-precursor-based (blue) routes. (f) Digital photo showing as-synthesised graphene on 12-inch  $\times$  4-inch-sized quartz in one batch. (g, h) Histogram of measured transmittance (g) and sheet resistance (h) over a 12-inch-sized graphene film. (a–e) Reproduced with permission.<sup>32</sup> Copyright 2016, Wiley-VCH. (f–h) Reproduced with permission.<sup>37</sup> Copyright 2023, Wiley-VCH.

Glass fibre fabric, a commercial material with high mechanical strength and flexibility, is widely used in structural reinforcements.<sup>65</sup> Combining graphene with glass fibre would enable cutting-edge applications, rendering it crucial to produce large-sized graphene glass fibre fabric (GGFF). Note that uneven thickness distributions of graphene films grown on large-area glass fibre materials were observed when using either methane or ethane as the carbon source (Figure 5a–5b), because of the significant difference in their decomposition barriers. To prepare large-sized GGFF with high graphene uniformity, Liu *et al.* proposed a strategy of using both methane and ethanol as complementary carbon sources (Figure 5c). At an optimal ethanol/methane ratio of 5:1, the D ( $1350\text{ cm}^{-1}$ ), G ( $1580\text{ cm}^{-1}$ ), and 2D ( $2700\text{ cm}^{-1}$ ) bands in Raman contour map for a  $40\text{ cm} \times 4\text{ cm}$ -sized GGFF show uniform colour contrast, demonstrating its good uniformity (Figure 5d). Furthermore, the sheet resistance mapping results from upstream to downstream also display noticeable enhancement in uniformity (Figure 5e).

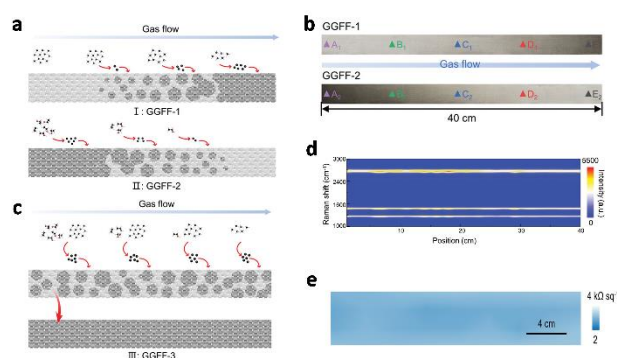


**Fig. 5** Uniform synthesis of large-scale GGFF composites using a mixed carbon source strategy. (a) Schematic diagram of GGFF preparation using methane (I, GGFF-1) and ethanol (II, GGFF-2) as the carbon source. (b) Photograph showing the growth results of GGFF-1 (upper panel) and GGFF-2 (lower panel). (c) Schematic diagram of GGFF preparation using mixed carbon sources. (d) Uniform colour contrast of Raman intensity of D ( $I_D$ ) ( $1350\text{ cm}^{-1}$ ), G ( $I_G$ ) ( $1580\text{ cm}^{-1}$ ), and 2D ( $I_{2D}$ ) ( $2700\text{ cm}^{-1}$ ) bands (collected along a lateral distance of  $40\text{ cm}$  from the sample centre axis, with a uniform spacing of  $1\text{ cm}$  between 41 points). (e) Sheet resistance mapping results of GGFF-3-3000 (with a uniform spacing of  $2\text{ cm}$  between two points, dimensions:  $40\text{ cm} \times 4\text{ cm}$ ). (a–e) Reproduced with permission.<sup>65</sup> Copyright 2022, Wiley-VCH.

### Transfer-free growth on inch-sized wafer substrates

Recently, 2 to 4-inch-sized graphene wafers with high uniformity have been obtained by introducing catalyst in a reasonable way or designing the substrate surface<sup>70,71</sup>. Sapphire wafers are widely used in LED industry as the preferred support for epitaxial growth of nitrides, thanks to their excellent mechanical properties, dielectric properties, chemical stability, and atomic smoothness.<sup>72,73</sup> However, because of the lattice and thermal mismatches between nitrides and the underlying sapphire, numerous threading dislocations in the epitaxial layer are difficult to be avoided. Graphene, when functioning as the interface layer between nitride and sapphire, can facilitate the elimination of these dislocations by promoting lateral 2D growth of nitrides.<sup>74</sup> The introduction of catalytic booster, either in the gas phase or on the sapphire substrate,<sup>75</sup> has been proven as efficient manoeuvre to obtain wafer-scale high-quality graphene on sapphire. As for the former, controlling the catalyst contents in the gas phase is vital to guarantee sufficient catalyst supply but to avoid metal residues on graphene surface.<sup>36</sup> Although copper vapours can

serve as atmospheric catalysts, this is uncontrollable due to the inability to regulate the rate of vapour generation. Shan *et al.* introduced a copper-containing precursor, copper acetate [ $\text{Cu}(\text{OAc})_2$ ], which could provide both Cu catalyst and carbon source simultaneously.<sup>36</sup> The Cu vapor content is precisely adjusted *via* heating the precursor to make it pre-decomposed in an independent low-temperature furnace placed upstream of the CVD system (Figure 6a–6c). Employing this strategy, a 2-inch-sized graphene/sapphire wafer with high transparency and good uniformity could be obtained (Figure 6d). Moreover, by introducing copper catalyst in the gas phase, the  $sp^3$  hybridisation content in graphene films is significantly reduced compared to those prepared without copper acetate (Figure 6e). Upon growth, no copper residues could be detected (Figure 6f). Raman characterisation confirmed improved quality of graphene (Figure 6g–6h) and atomic force microscopy inspections further verified reduced multilayer graphene content (Figure 6i). Moreover, this method exhibits high practicability to directly grow graphene on other insulating substrates.

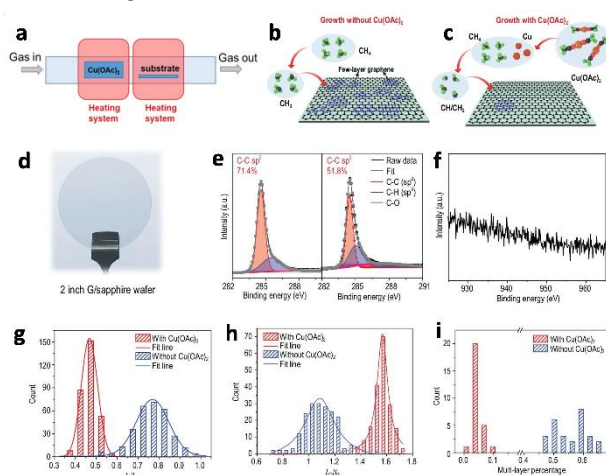


**Fig. 6** Synthesis of wafer-sized graphene using  $\text{Cu}(\text{OAc})_2$ -assisted strategy. (a) Schematic diagram of the pre-decomposition CVD reaction system. (b, c) Schematic diagrams of graphene growth process without (left) and with (right)  $\text{Cu}(\text{OAc})_2$ . (d) Photograph of one piece of 2-inch-sized graphene/sapphire wafer. (e) XPS C1s spectra of graphene grown with (left) and without (right)  $\text{Cu}(\text{OAc})_2$ . (f) XPS spectra, without observation of Cu  $2p_{3/2}$  signal, indicating the absence of copper species. (g, h) Statistics of  $I_D/I_G$  (g) and intensity ratio of Raman 2D to G band ( $I_{2D}/I_G$ ) (h) with (red) and without (blue)  $\text{Cu}(\text{OAc})_2$ . (i) Percentage of multilayer graphene grown with (red) and without (blue)  $\text{Cu}(\text{OAc})_2$ . (a–i) Reproduced with permission.<sup>36</sup> Copyright 2022, Science China Press.

$\text{Cu}(111)$  film deposited on  $\text{Al}_2\text{O}_3(0001)$  wafer has also been utilised to aid in the transfer-free growth of monolayer graphene on sapphire substrates (Figure 7a).<sup>75</sup> To obtain single-crystal  $\text{Cu}(111)$  tightly adhered to the substrate, commercial polycrystalline copper foil is placed on the sapphire substrate and heated for an extended period at a temperature close to the melting point of copper. After that, methane was introduced as carbon source to grow graphene. Multi-cycle plasma etching (MPE) was used every 30 min to remove graphene on Cu surface that was grown following a "surface self-limiting" mechanism, so that the active carbon species can diffuse to the Cu/sapphire interface. The low carbon solubility of Cu hinders the segregation process, resulting in a lower graphene growth rate on the Cu/sapphire interface than that on the Cu surface. After the growth process is completed, the sample is immersed in liquid nitrogen for a while, then rapidly heated so that the expanding of

nitrogen between the copper film and sapphire could cause the copper film to be easily peeled off, ultimately obtaining a perfect sapphire-based graphene sample (Figure 7b). Low energy electron diffraction patterns obtained throughout the entire measured sample area were uniform to display a singular hexagonal structure, supporting the growth of single-crystal graphene.

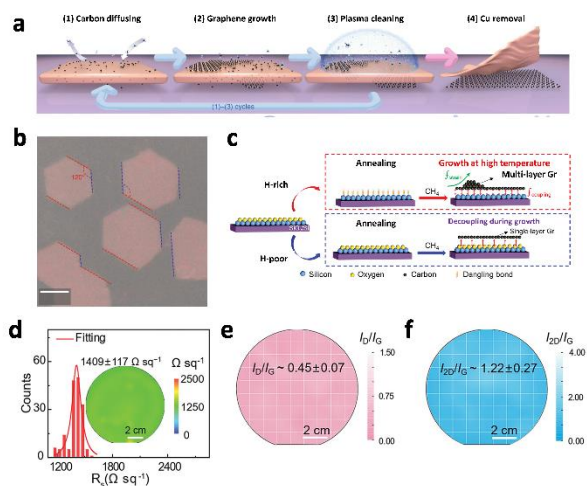


**Fig. 7** Synthesis of wafer-sized transfer-free graphene films based on pre-treatment of the substrates. (a) Schematic illustrating the graphene growth process during MPE-CVD. (b) Optical microscopy image showing graphene islands formed on  $\text{Al}_2\text{O}_3(0001)$ . (c) Schematic demonstrating the low-hydrogen decoupling strategy employed for graphene growth on silicon wafer surfaces. (d) Statistical histogram of sheet resistance for 4-inch-sized graphene/Si wafers, accompanied by corresponding spatial distribution maps. (e, f)  $I_D/I_G$  (e) and  $I_{2D}/I_G$  (f) maps of a 4-inch-sized graphene/Si wafer. (a, b) Reproduced with permission.<sup>75</sup> Copyright 2022, Springer Nature. (c-f) Reproduced with permission.<sup>64</sup> Copyright 2022, Wiley-VCH.

Silicon wafers are extensively used across a wide range of chip manufacturing processes.<sup>76, 77</sup> Compared to graphene/sapphire materials, which could be utilised for the fabrication of blue-light LEDs<sup>78</sup> and cater to devices that require high power density, graphene/silicon wafers are more suitable for producing large-scale LED chips even in peelable type.<sup>79</sup> However, silicon features a higher density of surface dangling bonds,<sup>80</sup> leading to stronger interfacial interactions with graphene. This facilitates the formation of dense, small-sized and multilayered graphene, *i.e.*, severe non-uniform growth behaviours. Ci *et al.* adopted an interface decoupling strategy to avoid the occurrence of the “Stranski–Krastanov” growth mode (Figure 7c) and obtained monolayer graphene on a 4-inch-sized silicon wafer.<sup>64</sup> This is due to the fact that the formation of silicon dangling bonds on the substrate is effectively minimised by reducing the use of hydrogen and introducing methanol into the reaction chamber. Moreover, the hydroxyl groups formed by the decomposition of methanol combine with silicon dangling bonds to form Si-OH groups, hydroxylating the substrate surface to weaken the interaction between graphene and substrate. Theoretical calculations showed that under hydroxyl termination, the binding energy is minimised, indicating that the interaction between graphene and the substrate is weakened, and their distance is maximised. Furthermore, the presence of hydroxyl groups can accelerate the decomposition of methane, contributing to the improvement of graphene quality. This significantly improves the smoothness and uniformity of the graphene film (Figure 7d–7f).

Taken together, Cu catalyst in the gas phase effectively improves graphene quality but becomes more challenging when further increase the substrate size, because of the stringent requirement on catalyst contents. Utilising Cu(111) as a buffer layer facilitates the growth of high-quality graphene on wafer-scale sapphire. Nevertheless, the sputtering and subsequent removal of the Cu buffer layer introduce extra process and cost – it is likely to impose limitations on the scalability. The “decoupling” strategy aims to achieve high-quality control by reducing the interaction between graphene and the substrate. However, its compatibility with other types of substrates needs to be evaluated. Innovative designs are still required to overcome these issues.

## Susceptor design in batch growth of transfer-free graphene

Upon developing rapid synthesis of large-area graphene with high film uniformity, grand challenges arise pertaining to preparing multiple pieces of graphene samples in one batch.<sup>81</sup> Among these, ensuring batch uniformity becomes an increasingly important subject and needs to be addressed when scaling graphene production from lab to fab. The key to achieving this goal is to guarantee the uniform distribution of carbon species above surface of each substrate.<sup>82</sup> However, for typical CVD systems, the distribution of both thermal and flow fields within the entire reaction chamber becomes unexpectedly inhomogeneous upon the sample loading. To solve this, the arrangement of substrates particularly the susceptor/holder design becomes crucial.

### Susceptor for producing large-area graphene film

Considering the dimension, plate/sheet substrates for graphene film growth are usually placed along the flow direction, that is, in parallel to the axial direction of the quartz tube. Liu *et al.* designed a susceptor that contains quartz plates parallel to the flow direction (Figure 8a).<sup>37</sup> By confining the hydroxyl groups generated from the quartz glass at high temperatures and the gas-phase substances within small gaps, they successfully promoted the preparation of high-quality graphene (Figure 8b). Five pieces of 12-inch-sized quartz glasses could be placed in the same batch using a reactor tube with a diameter of 6 inch (Figure 8c), which can be further extended by using larger CVD chambers. In this work, the effect of the microfluidic field at the substrate interface on the quality of graphene growth determines the optimal arrangement gap between the two pieces of substrates (Figure 8d–8e). The results showed that, when the gap is 20 nm, a uniform carbon-active molecular flow is formed between the two pieces (Figure 8f), ensuring the uniformity of the large-size graphene film. In addition, hydroxyl groups can significantly reduce the energy barrier for methane decomposition and thus increase graphene growth rate.<sup>83</sup> Using this experimental strategy, a

production of 5 pieces of 12-inch-sized graphene films on quartz glass could be attained (Figure 8g–8i).

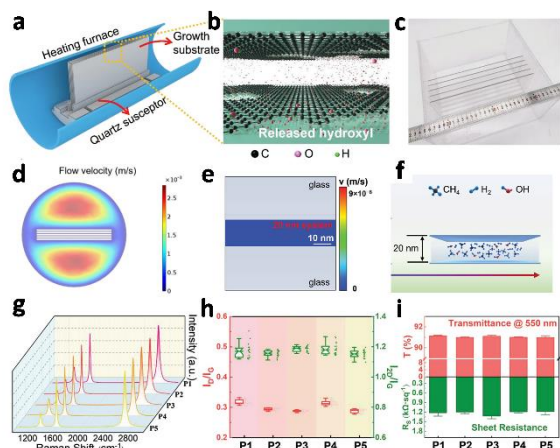


**Fig. 8** Susceptor design for the batch production of 12-inch-sized quartz sheets. (a) Schematic illustration of the batch production of graphene on glass sheets. (b) Schematic illustration of the dihydroxylation process of the quartz substrate. (c) Photograph showing 5 pieces of 12-inch  $\times$  4-inch-sized graphene on quartz substrate in one batch. (d) Computational fluid dynamics (CFD) simulations of local distribution of flow rate in the reaction system, with significant difference inside and outside the microflow reactor. (e) CFD simulations of gas velocity distributions in the 20 nm gap distance. (f) Schematic illustrating the microflow in the gap with 20 nm gap distances. (g) Raman spectra (with normalised G peak intensity) of the as-synthesised graphene. (h) Statistical results of  $I_D/I_G$  and  $I_{2D}/I_G$  of the 5 samples in (c). (i) Average transmittance and sheet resistance of the 5 samples in (c). (a–i) Reproduced with permission.<sup>37</sup> Copyright 2023, Wiley-VCH.

### Susceptor for producing large-area graphene wafer

Considering that the wafer substrates and quartz tubes have circular cross-sections, the arrangement of wafer substrates is usually different from those of plates/sheets to boost the production capacity of one batch. Jiang *et al.* used a specially designed susceptor to place 4-inch-sized quartz wafers perpendicular to the gas flow direction and successfully produced 30 pieces of graphene wafers in one batch.<sup>31</sup> Figure 9a shows the computational fluid dynamics simulation of the carrier's internal flow field using finite element analysis. Based on the results obtained for different spacing values between adjacent wafers, the optimal one was determined to be 10 mm and 15 mm (Figure 9c). The airflow diagram in Figure 9b shows small vortices at the edges of each wafer, the presence of which ensures a limited reaction space between adjacent wafers, and thus guaranteeing the uniform growth of wafer-level graphene films (Figure 9d). In particular, the heating system was optimised to ensure uniform temperature distribution throughout the CVD reaction, precisely adjusted the flow speed and direction to ensure uniform and stable gas distribution, and optimised the gas environment by adjusting the types and ratios of reaction gases (Figure 9e–9f). These efforts have enabled successful preparation of uniform graphene on different types of insulators, laying the foundation for batch production and applications of graphene wafers.

Despite the fruitful progresses realized in transfer-free CVD growth of large-area and high-quality graphene on insulating substrates,<sup>37, 32</sup> there has been a clear lack of equipment construction to date for

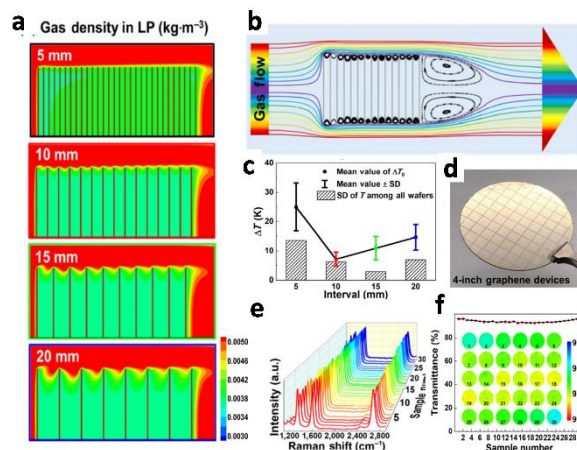


**Fig. 9** Batch production of graphene wafers. (a) Gas density distribution of wafers with different spacings in the LPCVD system. (b) Flow field distribution in the LPCVD system. (c) Graph depicting the uniformity of thermal fields within the wafers. (d) Photograph of 4-inch-sized graphene devices. (e) Raman spectra of as-grown wafers with normalised G peak. (f) Average transmittance of the as-grown graphene wafers and their maps (inset). (a–f) Reproduced with permission.<sup>31</sup> Copyright 2020, Springer Nature.

### Equipment construction toward scalable production of transfer-free graphene

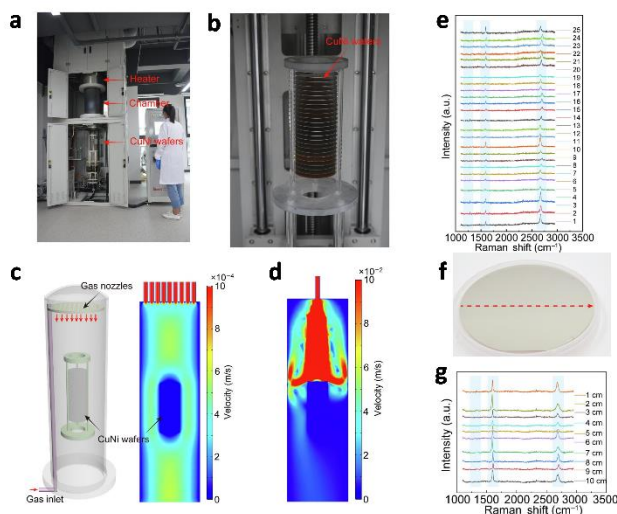


**Fig. 10** Equipment construction for production of wafer-scale graphene. (a) Pilot-scale APCVD furnace for growing single-crystal graphene on CuNi(111)/sapphire wafers. (b) Photograph of the susceptor designed to contain 25 pieces of CuNi(111)/sapphire wafers used for graphene growth. (c) 3D image showing the positions of CuNi wafers inside the CVD furnace (left) and corresponding flow fields distribution with the gas homogeniser (right). (d) Simulated gas velocity distribution with a single nozzle. (e) Raman spectra of graphene grown on 25 pieces of CuNi(111)/sapphire wafers from the same batch. (f) Photograph of one piece of graphene/CuNi(111) wafer. (g) Raman spectra of graphene grown on CuNi(111) wafers at different locations in (f). (a–g) Reproduced with permission.<sup>16</sup> Copyright 2019, Science China Press.

scalable production of transfer-free graphene films. In this section, equipment and techniques developed for the scalable production of graphene on metal substrates and other layered materials on

insulating substrates will be described, which offers a hint to address the key points for equipment design toward scalable production of transfer-free graphene.

From the perspective of macroscopic design, the required size and productivity of graphene determine the chamber size of the CVD reactor, which further impacts the equipment dimension. For instance, the reported maximum size of layered materials was 25 inches.<sup>32</sup> In addition, whether the CVD furnace is placed vertically or horizontally need to be considered, especially when heavy susceptors loaded with multiple samples needs to be transferred at a high temperature and in a low-pressure chamber. This is also related with the design of flow/thermal field, as well as the evaluation of gravity influence. Deng *et al.* reported fast production of 25 pieces of 4-inch-sized graphene on Cu<sub>90</sub>Ni<sub>10</sub>(111) wafers using a custom-built vertical furnace.<sup>16</sup> The key design of this equipment includes a vertical sampling stage for the Cu<sub>90</sub>Ni<sub>10</sub> wafers (Figure 10a-10b) and a chamber with multiple gas inlets to ensure uniform gas flow throughout the chamber (Figure 10c and 10d). This equipment synergizes large-scale productivity and gas-phase reaction stability. As a result, batch uniformity was achieved, as indicated by the absence of D peak in Raman spectra of a group of 25 graphene wafers

(Figure 10e). Moreover, synthesis uniformity within one individual wafer was also realized using this equipment (Figure 10f-10g).

The heating modes of a CVD equipment need to be considered in terms of production cost, sample size, and product capacity. Susceptors aforementioned were placed in quartz tube in hot-wall CVD (HW-CVD) furnaces, for which the heating region covers the entire chamber.<sup>63</sup> However, both the temperature extremes (e.g., 1150 °C) and chamber volumes are limited by the quartz materials, in close relation to its melting point and manufacture difficulty. In contrast, as for a CW-CVD reactor, the heating region is merely confined at the substrate, which allows the substrate to reach higher temperatures and requires less energy consumption. In addition, quartz tubes could be replaced by other materials, which further increase the size of produced graphene films. In particular, electromagnetic induction is one of the applicable methods to guarantee a uniform temperature distribution on the substrate surface, as evidenced by Chen *et al.* However, susceptors for CW-CVD furnaces usually need to be produced by materials with elevated heat conductivity, which might be more challenging in comparison with the HW-CVD. The uniqueness of the substrates, such as surface chemistry, also requests consideration, as it might result in diverse behaviours at high temperatures.

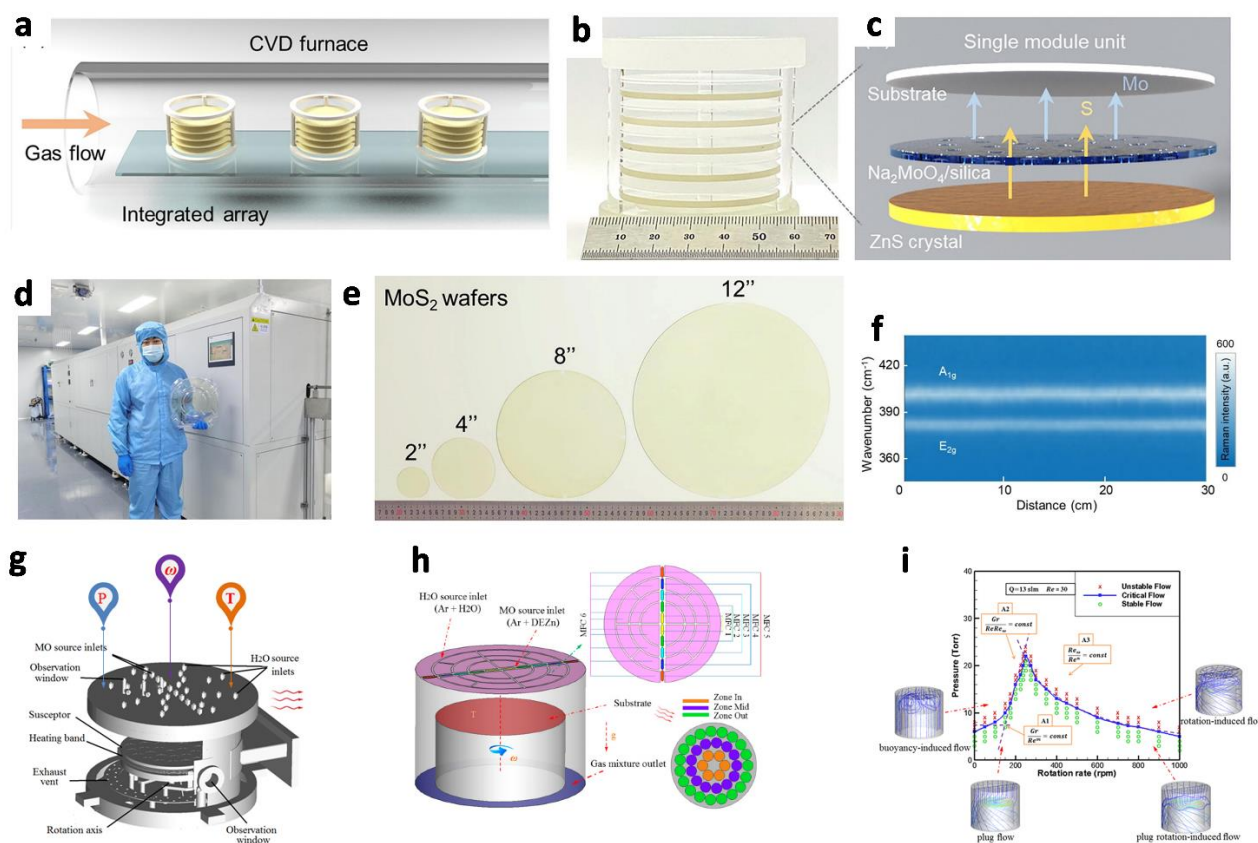


**Fig. 11** Equipment construction for scalable production of other 2D materials. (a) Schematic of module design for large-scale production of 15 pieces of MoS<sub>2</sub> wafers. (b) Photograph of an integrated array consisting of five stacked 2-inch-sized production module units from (a). (c) Schematic of a single module unit from (b). (d) Custom-automated CVD furnace equipped with a quartz tube with a diameter of 350 mm. (e) Photograph of uniform MoS<sub>2</sub> thin films on 2- to 12-inch-sized sapphire wafers. (f) Raman line map along the horizontal axis of a 12-inch MoS<sub>2</sub> wafer. (g) 3D model of a prototype reactor for zinc oxide metal-organic chemical vapor deposition (ZnO-MOCVD). (h) Computational fluid dynamics simulation of the ZnO-MOCVD model and chip distribution on the substrate surface. (i) Stability P- $\omega$  plot of the ZnO-MOCVD reactor. (a-f) Reproduced with permission.<sup>85</sup> Copyright 2023, Science China Press. (g-i) Reproduced with permission.<sup>86</sup> Copyright 2019, MDPI.

The uniform and stable delivery of gases within the reaction system is crucial for the scalable production of transfer-free graphene, which is in analogous to the requirements for producing other 2D materials (MoS<sub>2</sub>, ZnO, and III-nitride).<sup>84</sup> In this respect, the design of substrate susceptor and flow homogeniser are of equal importance. It is worth noting that the distribution of thermal fields would also influence the flow field, especially in the CW-CVD system.<sup>53</sup> Moreover, guaranteeing a uniform flow field will be more challenging when liquid or solid precursors are used, where the precise adjustment of temperature, gas flow and chamber pressure could be useful.

To envisage the improved productivity and size diversity of graphene directly grown on insulating substrates, multiple module integration would also be a key. Xue *et al.* designed and customised an automated CVD reactor with a tube diameter of 350 mm (Figure 11a–11d),<sup>85</sup> based on which a single batch can produce 10 pieces of 4-inch-sized wafers, 5 pieces of 8-inch-sized wafers, or 3 pieces of 12-inch-sized wafers. These produced monolayer MoS<sub>2</sub> all exhibit high optical uniformity (Figure 11e). Especially, the excellent material uniformity of 12-inch-sized wafers was verified through large-scale Raman linear scanning (Figure 11f). Notably, this automated CVD equipment supports up to four cycles of synthesis per day, endowing it with a strong capability for mass production. In further contexts, utilising theoretical calculation and artificial intelligence would help reduce the costs of manpower, resources and time to a certain extent.<sup>86–91</sup> Li *et al.* established a transport reaction model for ZnO growth using diethylzinc and H<sub>2</sub>O through theoretical calculations, based on a MD600B ZnO-MOCVD system as a prototype (Figure 11g).<sup>86</sup> The key of this model lies in controlling the supply rate of Zn source through five independent mass flow controllers (Figure 11h) to ensure the fine distribution of sources above each wafer, thereby guaranteeing the consistency of the film uniformity of each wafer's final epitaxy. H<sub>2</sub>O was controlled by a separate mass flow controller, and the high-speed rotating substrate holder further offered uniform gas distribution above each wafer track, ultimately preparing a nice ZnO film on the target substrate. The model also discusses four different flow states under different working conditions: buoyancy-induced flow, plug flow, plug rotation-induced flow, and rotation-induced flow. The calculation results, as shown in Figure 11i, indicate that plug flow and plug rotation-induced flow are more stable, while the buoyancy-induced flow and rotation-induced flow are unstable. Such a study is also meaningful for the selection of growth parameters in scalable production of transfer-free graphene films. It provides a specific growth process window to maintain laminar flow stability, narrow the debugging range, and save the operational time.

## Conclusion and prospects

This review first proposes the existing challenges toward the batch production of transfer-free graphene on insulating substrates, including lengthy preparation time, small sample sizes, poor piece-to-batch uniformity, and equipment deficiency for scalable production. It follows the comprehensive summary on the recent advances in designing strategies to solve these issues. Our insight into the development of growth routes and related scalable production equipment are further provided, aiming to facilitate the batch production of transfer-free graphene and their practical applications.

Depending on the application scenarios, different types of substrates need to be employed, followed by utilising suitable preparation methods of transfer-free graphene. Future research efforts should be focused upon the technological innovation to achieve cost-effective and quality-controllable graphene production on insulating substrates. This might involve developing new equipment adapted to the features of different insulating substrates. For example, as for sapphire substrates with high temperature tolerance, the development of electromagnetic induction CVD equipment could be considered, ensuring the preparation of high-quality graphene films with favourable production efficiency. In terms of quartz and silicon substrates, ensuring uniformity in thermal/flow fields and gas-phase reaction environments otherwise requests the design of suitable batch susceptors.

In addition, during the process of industrial-level production of graphene with the employment of elevated temperatures and flammable/explosive gases (methane, acetylene, and hydrogen gases), it is crucial to ensure the operational safety. Key safety measures should include, but not limited to, adopting explosion-proof equipment design with automatic shutdown systems to prevent gas leakage, deploying gas detection and efficient ventilation systems in critical production areas, and developing comprehensive emergency response plan coupled with regular safety training. These measures are fundamental to guarantee the industrial safety of producing graphene, helping reduce the risk of related accidents.

Overall, with continuous strategic proposal and equipment upgrading, large-scale production of transfer-free graphene films is expected to provide a more reliable material foundation, and thus facilitate the transition from lab-scale fundamental research to industrial-level applications.

## Conflicts of interest

There are no conflicts to declare.

## Acknowledgements

This work was supported by the National Key R&D Program of China (2019YFA0708204), National Natural Science Foundation of China (T2188101), Science Fund for Distinguished Young Scholars of Jiangsu Province (BK20211503), and Jiangsu Funding Program for Excellent Postdoctoral Talent (2022ZB595).

## Notes and references

- 1 A. Tyagi, V. Mišeikis, L. Martini, S. Forti, N. Mishra, Z. M. Gebeyehu, M. A. Giambra, J. Zribi, M. Frégnaux and D. Aureau, *Nanoscale*, 2022, **14**, 2167-2176.
- 2 N. Petrone, C. R. Dean, I. Meric, A. M. Van Der Zande, P. Y. Huang, L. Wang, D. Muller, K. L. Shepard and J. Hone, *Nano Lett.*, 2012, **12**, 2751-2756.
- 3 K. S. Novoselov, A. K. Geim, S. V. Morozov, D. e. Jiang, Y. Zhang, S. V. Dubonos, I. V. Grigorieva and A. A. Firsov, *Science*, 2004, **306**, 666-669.
- 4 F. Bonaccorso, Z. Sun, T. Hasan and A. C. Ferrari, *Nat. Photonics*, 2010, **4**, 611-622.
- 5 D. Akinwande, C. Huyghebaert, C. H. Wang, M. I. Serna, S. Goossens, L. J. Li, H. S. P. Wong and F. H. Koppens, *Nature*, 2019, **573**, 507-518.
- 6 Z. Chen, Y. Qi, X. Chen, Y. Zhang and Z. Liu, *Adv. Mater.*, 2019, **31**, 1803639.
- 7 Z. Chen, X. Zhang, Z. Dou, T. Wei, Z. Liu, Y. Qi, H. Ci, Y. Wang, Y. Li, H. Chang, J. Yan, S. Yang, Y. Zhang, J. Wang, P. Gao, J. Li and Z. Liu, *Adv. Mater.*, 2018, **30**, 1801608.
- 8 Z. Chen, P. Gao and Z. Liu, *Acta. Phys. Chim. Sin.*, 2020, **36**, 1907004.
- 9 H. Ci, H. Ren, Y. Qi, X. Chen, Z. Chen, J. Zhang, Y. Zhang and Z. Liu, *Nano Res.*, 2018, **11**, 3106-3115.
- 10 M. Juvaidd, S. Sarkar, P. K. Gogoi, S. Ghosh, M. Annamalai, Y.-C. Lin, S. Prakash, S. Goswami, C. Li and S. Hooda, *ACS Nano*, 2020, **14**, 3290-3298.
- 11 C. Berger, Z. Song, X. Li, X. Wu, N. Brown, C. Naud, D. Mayou, T. Li, J. Hass and A. N. Marchenkov, *Science*, 2006, **312**, 1191-1196.
- 12 X. Li, W. Cai, J. An, S. Kim, J. Nah, D. Yang, R. Piner, A. Velamakanni, I. Jung, E. Tutuc, S. K. Banerjee, L. Colombo and R. S. Ruoff, *Science*, 2009, **324**, 1312-1314.
- 13 A. Reina, X. Jia, J. Ho, D. Nezich, H. Son, V. Bulovic, M. S. Dresselhaus and J. Kong, *Nano Lett.*, 2009, **9**, 30-35.
- 14 K. S. Novoselov, L. Colombo, P. Gellert, M. Schwab and K. Kim, *Nature*, 2012, **490**, 192-200.
- 15 V. L. Nguyen and Y. H. Lee, *Small*, 2015, **11**, 3512-3528.
- 16 B. Deng, Z. Xin, R. Xue, S. Zhang, X. Xu, J. Gao, J. Tang, Y. Qi, Y. Wang, Y. Zhao, L. Sun, H. Wang, K. Liu, M. H. Rummeli, L.-T. Weng, Z. Luo, L. Tong, X. Zhang, C. Xie, Z. Liu and H. Peng, *Sci. Bull.*, 2019, **64**, 659-668.
- 17 A. Alazmi, S. Rasul, S. P. Patole and P. M. Costa, *Polyhedron*, 2016, **116**, 153-161.
- 18 F. La Via, M. Camarda and A. La Magna, *Appl. Phys. Rev.*, 2014, **1**, 031301.
- 19 K. Yan, L. Fu, H. Peng and Z. Liu, *Acc. Chem. Res.*, 2013, **46**, 2263-2274.
- 20 R. Munoz and C. Gómez - Aleixandre, *Chem. Vap. Deposition.*, 2013, **19**, 297-322.
- 21 X. Li, L. Colombo and R. S. Ruoff, *Adv. Mater.*, 2016, **28**, 6247-6252.
- 22 H. Tetlow, J. P. De Boer, I. J. Ford, D. D. Vvedensky, J. Coraux and L. Kantorovich, *Phys. Rep.*, 2014, **542**, 195-295.
- 23 Y. Chen, X. L. Gong and J. G. Gai, *Adv. Sci.*, 2016, **3**, 1500343.
- 24 Y. Zhu, J. Zhang, T. Cheng, J. Tang, H. Duan, Z. Hu, J. Shao, S. Wang, M. Wei, H. Wu, A. Li, S. Li, O. Balci, S. M. Shinde, H. Ramezani, L. Wang, L. Lin, A. C. Ferrari, B. I. Yakobson, H. Peng, K. Jia and Z. Liu, *Adv. Mater.*, DOI: 10.1002/adma.202308802.
- 25 B. Liu and S. Ma, *Nanoscale*, 2024, **16**, 4407-4433.
- 26 J. Shan, L. Cui, F. Zhou, R. Wang, K. Cui, Y. Zhang and Z. Liu, *ACS Appl. Mater. Interfaces.*, 2020, **12**, 11972-11978.
- 27 S. Wei, L. Ma, M.-L. Chen, Z. Liu, W. Ma, D. Sun, H. Cheng and W. Ren, *Carbon*, 2019, **148**, 241-248.
- 28 B. Liu, H. Wang, W. Gu, L. Zhou, Z. Chen, Y. Nie, C. Tan, H. Ci, N. Wei, L. Cui, X. Gao, J. Sun, Y. Zhang and Z. Liu, *Nano Res.*, 2021, **14**, 260-267.
- 29 S. Tang, H. Wang, H. S. Wang, Q. Sun, X. Zhang, C. Cong, H. Xie, X. Liu, X. Zhou, F. Huang, X. Chen, T. Yu, F. Ding, X. Xie and M. Jiang, *Nat. Commun.*, 2015, **6**, 6499.
- 30 X. D. Chen, Z. Chen, W. S. Jiang, C. Zhang, J. Sun, H. Wang, W. Xin, L. Lin, M. K. Priyadarshi, H. Yang, Z. B. Liu, J. G. Tian, Y. Zhang, Y. Zhang and Z. Liu, *Adv. Mater.*, 2017, **29**, 1603428.
- 31 B. Jiang, Q. Zhao, Z. Zhang, B. Liu, J. Shan, L. Zhao, M. H. Rummeli, X. Gao, Y. Zhang, T. Yu, J. Sun and Z. Liu, *Nano Res.*, 2020, **13**, 1564-1570.
- 32 X. D. Chen, Z. L. Chen, W. S. Jiang, C. H. Zhang, J. Y. Sun, H. H. Wang, W. Xin, L. Lin, P. K. Manish, H. Yang, *Adv. Mater.*, 2016, **29**, 1603428.
- 33 J. Shan, J. Sun and Z. Liu, *ChemNanoMat*, 2021, **7**, 515-525.
- 34 X. Gao, S. Li, J. Bi, K. Zhou, M. Li, Z. Liu and J. Sun, *Sci. China Chem.*, 2023, **67**, 824-840.
- 35 Y. Li, K. Zhou, H. Ci and J. Sun, *ChemSusChem*, 2023, **16**, e202300865.
- 36 J. Shan, S. Fang, W. Wang, W. Zhao, R. Zhang, B. Liu, L. Lin, B. Jiang, H. Ci, R. Liu, W. Wang, X. Yang, W. Guo, M. H. Rummeli, W. Guo, J. Sun and Z. Liu, *Natl. Sci. Rev.*, 2022, **9**, nwab169.
- 37 B. Liu, Z. Sun, K. Cui, Z. Xue, Z. Li, W. Wang, W. Gu, K. Zheng, R. Liu, Y. Zhao, M. H. Rummeli, X. Gao, J. Sun and Z. Liu, *Adv. Funct. Mater.*, 2023, **33**, 2210771.
- 38 X. D. Chen, Z. L. Chen, J. Y. Sun, Y. F. Zhang and Z. F. Liu, *Acta. Phys. Chim. Sin.*, 2016, **32**, 14-27.
- 39 Z. Chen, B. Guan, X. d. Chen, Q. Zeng, L. Lin, R. Wang, M. K. Priyadarshi, J. Sun, Z. Zhang, T. Wei, J. Li, Y. Zhang, Y. Zhang and Z. Liu, *Nano Res.*, 2016, **9**, 3048-3055.
- 40 M. A. Fanton, J. A. Robinson, C. Puls, Y. Liu, M. J. Hollander, B. E. Weiland, M. LaBella, K. Trumbull, R. Kasarda, C. Howsare, J. Stitt and D. W. Snyder, *ACS Nano*, 2011, **5**, 8062-8069.
- 41 C. Thierfelder, M. Witte, S. Blankenburg, E. Rauls and W. Schmidt, *Surf. Sci.*, 2011, **605**, 746-749.
- 42 X. Li, C. W. Magnuson, A. Venugopal, R. M. Tromp, J. B. Hannon, E. M. Vogel, L. Colombo and R. S. Ruoff, *J. Am. Chem. Soc.*, 2011, **133**, 2816-2819.
- 43 Z. Dong, B. Li, C. Cui, W. Qian, Y. Jin and F. Wei, *React. Chem. Eng.*, 2020, **5**, 991-1004.
- 44 X. Cui, H. Li, Y. Wang, Y. Hu, L. Hua, H. Li, X. Han, Q. Liu, F. Yang, L. He, X. Chen, Q. Li, J. Xiao, D. Deng and X. Bao, *Chem*, 2018, **4**, 1902-1910.
- 45 A. Luntz and D. Bethune, *J. Chem. Phys.*, 1989, **90**, 1274-1280.
- 46 L. Juurlink, D. Killelea and A. Utz, *Prog. Surf. Sci.*, 2009, **84**, 69-134.
- 47 M. S. Liao and Q. E. Zhang, *J. Mol. Catal. A: Chem.*, 1998, **136**, 185-194.
- 48 Z. Chen, C. Xie, W. Wang, J. Zhao, B. Liu, J. Shan, X. Wang, M. Hong, L. Lin, L. Huang, X. Lin, S. Yang, X. Gao, Y. Zhang, P. Gao, K. Novoselov, J. Sun and Z. Liu, *Sci. Adv.*, 2021, **7**, eabk0115.
- 49 X. Sun, L. Lin, L. Sun, J. Zhang, D. Rui, J. Li, M. Wang, C. Tan, N. Kang, D. Wei, H. Q. Xu, H. Peng and Z. Liu, *Small*, 2018, **14**, 1702916.
- 50 M. Min, S. Seo, Y. Yoon, K. Cho, S. M. Lee, T. Lee and H. Lee, *Nanoscale*, 2016, **8**, 17022-17029.

- 51 F. Cuccureddu, S. Murphy, I. Shvets, M. Porcu, H. Zandbergen, N. Sidorov and S. Bozhko, *Surf. Sci.*, 2010, **604**, 1294-1299.
- 52 P. R. Ribič and G. Bratina, *Surf. Sci.*, 2007, **601**, 44-49.
- 53 K. Jia, H. Ci, J. Zhang, Z. Sun, Z. Ma, Y. Zhu, S. Liu, J. Liu, L. Sun, X. Liu, J. Sun, W. Yin, H. Peng, L. Lin and Z. Liu *Angew. Chem. Int. Ed.*, 2020, **132**, 17367-17371.
- 54 M. Yang, S. Sasaki, M. Ohnishi, K. Suzuki and H. Miura, *Jpn. J. Appl. Phys.*, 2016, **55**, 04EP05.
- 55 C. S. Chen and C. K. Hsieh, *Thin Solid Films*, 2015, **584**, 265-269.
- 56 G. Faggio, G. Messina, C. Lofaro, N. Lisi and A. Capasso, *C*, 2020, **6**, 14.
- 57 G. Faggio, A. Capasso, G. Messina, S. Santangelo, T. Dikonimos, S. Gagliardi, R. Giorgi, V. Morandi, L. Ortolani and N. Lisi, *J. Phys. Chem. C*, 2013, **117**, 21569-21576.
- 58 J. Pang, R. G. Mendes, P. S. Wrobel, M. D. Wlodarski, H. Q. Ta, L. Zhao, L. Giebeler, B. Trzebicka, T. Gemming, L. Fu, Z. Liu, J. Eckert, A. Bachmatiuk and M. H. Rummeli, *ACS Nano*, 2017, **11**, 1946-1956.
- 59 H. Wang, X. Xue, Q. Jiang, Y. Wang, D. Geng, L. Cai, L. Wang, Z. Xu and G. Yu, *J. Am. Chem. Soc.*, 2019, **141**, 11004-11008.
- 60 J. Chen, Y. Wen, Y. Guo, B. Wu, L. Huang, Y. Xue, D. Geng, D. Wang, G. Yu and Y. Liu, *J. Am. Chem. Soc.*, 2011, **133**, 17548-17551.
- 61 L. Tan, M. Zeng, Q. Wu, L. Chen, J. Wang, T. Zhang, J. Eckert, M. H. Rummeli and L. Fu, *Small*, 2015, **11**, 1840-1846.
- 62 Z. Chen, H. Chang, T. Cheng, T. Wei, R. Wang, S. Yang, Z. Dou, B. Liu, S. Zhang, Y. Xie, Z. Liu, Y. Zhang, J. Li, F. Ding, P. Gao and Liu, *Zhongfan, Adv. Funct. Mater.*, 2020, **30**, 2001483.
- 63 B. Jiang, D. Liang, Z. Sun, H. Ci, B. Liu, Y. Gao, J. Shan, X. Yang, M. H. Rummeli, J. Wang, T. Wei, J. Sun and Liu, *Zhongfan, Adv. Funct. Mater.*, 2022, **32**, 2200428.
- 64 H. Ci, J. Chen, H. Ma, X. Sun, X. Jiang, K. Liu, J. Shan, X. Lian, B. Jiang, R. Liu, B. Liu, G. Yang, W. Yin, W. Zhao, L. Huang, T. Gao, J. Sun and L. Zhongfan, *Adv. Mater.*, 2022, **34**, 2206389.
- 65 R. Liu, H. Yuan, J. Li, K. Huang, K. Wang, Y. Cheng, S. Cheng, W. Li, J. Jiang, C. Tu, Y. Qi and Liu, *Zhongfan, Small Methods*, 2022, **6**, 2200499.
- 66 Z. Li, W. Zhang, X. Fan, P. Wu, C. Zeng, Z. Li, X. Zhai, J. Yang and J. Hou, *J. Phys. Chem. C*, 2012, **116**, 10557-10562.
- 67 J. Sun, Y. Chen, M. K. Priyadarshi, Z. Chen, A. Bachmatiuk, Z. Zou, Z. Chen, X. Song, Y. Gao, M. H. Rummeli, Y. Zhang and Liu, *Zhongfan, Nano Lett.*, 2015, **15**, 5846-5854.
- 68 M. Hasan, W. Meiou, L. Yulian, S. Ullah, H. Q. Ta, L. Zhao, R. G. Mendes, Z. P. Malik, N. M. Ahmad, Z. Liu and R. M. H., *RSC Adv.*, 2019, **9**, 13527-13532.
- 69 Z. Chen, X. Guo, L. Zhu, L. Li, Y. Liu, L. Zhao, W. Zhang, J. Chen, Y. Zhang and Y. Zhao, *J. Mater. Sci. Technol.*, 2018, **34**, 1919-1924.
- 70 H. Ago, Y. Ogawa, M. Tsuji, S. Mizuno and H. Hibino, *J. Phys. Chem. Lett.*, 2012, **3**, 2228-2236.
- 71 F. Qing, C. Shen, R. Jia, L. Zhan and X. Li, *MRS Bull.*, 2017, **42**, 819-824.
- 72 S. J. Chang, Y. C. Lin, Y. K. Su, C. Chang, T. C. Wen, S. C. Shei, J. Ke, C. Kuo, S. Chen and C. Liu, *Solid State Electron.*, 2003, **47**, 1539-1542.
- 73 H. Tang, H. Li and J. Xu, *Advanced Topics on Crystal Growth[M]*. Rijeka: IntechOpen, 2013: 307-333.
- 74 H. Chang, Z. Liu, S. Yang, Y. Gao, J. Shan, B. Liu, J. Sun, Z. Chen, J. Yan, Z. Liu, J. Wang, P. Gao, J. Li, Z. Liu and T. Wei, *Light Sci. Appl.*, 2022, **11**, 88.
- 75 J. Li, M. Chen, A. Samad, H. Dong, A. Ray, J. Zhang, X. Jiang, U. Schwingenschlögl, J. Domke and C. Chen, *Nat. Mater.*, 2022, **21**, 740-747.
- 76 C. Mo, W. Fang, Y. Pu, H. Liu and F. Jiang, *J. Cryst. Growth.*, 2005, **285**, 312-317.
- 77 J. Wang and Y. Long, *Sci. Bull.*, 2018, **63**, 1267-1310.
- 78 M. Yamada, T. Mitani, Y. Narukawa, S. Shioji, I. Niki, S. Sonobe, K. Deguchi, M. Sano and T. Mukai, *Jpn. J. Appl. Phys.*, 2002, **41**, L1431.
- 79 S. Zhou, H. Xu, B. Tang, Y. Liu, H. Wan and J. Miao, *Opt. Express.*, 2019, **27**, A1506-A1516.
- 80 R. M. Lin, Y. C. Lu, S. F. Yu, Y. S. Wu, C. H. Chiang, W. C. Hsu and S. J. Chang, *J. Electrochem. Soc.*, 2009, **156**, H874.
- 81 Y. Zhang, D. Huang, Y. Duan, H. Chen, L. Tang, M. Shi, Z. Li and H. Shi, *Nanotechnology*, 2020, **32**, 105603.
- 82 A. N. Obraztsov, *Nat. Nanotechnol.*, 2009, **4**, 212-213.
- 83 M. Feng, X. Z. Jiang and K. H. Luo, *Proc. Combust. Inst.*, 2019, **37**, 5473-5480.
- 84 Y. Zhu, Z. Shi, Y. Zhao, S. Bu, Z. Hu, J. Liao, Q. Lu, C. Zhou, B. Guo, M. Shang, F. Li, Z. Xu, J. Zhang, Q. Xie, C. Li, X. Zhang, Z. Liu, L. Lin, P. Sun and B. Mao, *Nanoscale*, DOI:10.1039/D3NR05626K.
- 85 G. Xue, X. Sui, P. Yin, Z. Zhou, X. Li, Y. Cheng, Q. Guo, S. Zhang, Y. Wen, Y. Zuo, C. Zhao, M. Wu, P. Gao, Q. Li, J. He, E. Wang, G. Zhang, C. Liu and K. Liu, *Sci. Bull.*, 2023, **68**, 1514-1521.
- 86 J. Li, Z. Wu, Y. Xu, Y. Pei and G. Wang, *Molecules*, 2019, **24**, 876.
- 87 L. Kadinski, V. Merai, A. Parekh, J. Ramer, E. Armour, R. Stall, A. Gurary, A. Galyukov and Y. Makarov, *J. Cryst. Growth*, 2004, **261**, 175-181.
- 88 S. Liu, S. Gu, S. Zhu, J. Ye, W. Liu, X. Zhou, R. Zhang, Y. Shi and Y. Zheng, *J. Cryst. Growth*, 2007, **299**, 303-308.
- 89 Y. C. Chuang and C. T. Chen, *J. Taiwan Inst. Chem. Eng.*, 2014, **45**, 254-267.
- 90 Z. Zhang, H. Fang, H. Yan, Z. Jiang, J. Zheng and Z. Gan, *Appl. Therm. Eng.*, 2015, **91**, 53-61.
- 91 Z. Zhang, H. Fang, Q. Yao, H. Yan and Z. Gan, *J. Cryst. Growth*, 2016, **454**, 87-95.